SUBSONIC FRICTIONAL CAVITATING PENETRATION OF A THIN RIGID BODY INTO AN ELASTIC MEDIUM

by Y. A. ANTIPOV[†]

(*Department of Mathematics, Louisiana State University Baton Rouge, LA* 70803*, USA*)

[Received 7 October 2017. Revise 21 January 2018. Accepted 27 January 2018]

Summary

Two model problems of plane elasticity on subsonic steady-state motion of a thin rigid body in an elastic medium are analyzed. Both models concern a finite body symmetric with respect to the plane of motion and assume that the body contacts with the surrounding medium according to the Coulomb friction law. The body, while moves, leaves a trailing semi-infinite crack-like cavity moving at the body speed. The first model also assumes that ahead of the body a finite crack-like cavity is formed, and it is moving at the same speed. The second model does not admit the existence of this finite cavity. Both problems reduce to two sequently solved Riemann–Hilbert problems with piece-wise constant coefficients. Analysis of the solution to these problems obtained by quadratures reveals that the normal and tangential traction components and the normal velocity are continuous for any point of separation of the medium from the body. A criterion for the separation point based on the analysis of the sign of the normal traction component is proposed. Numerical results for the length of the fore crack (the first model), the normal traction and the resistance force for some ogive-nose penetrators are reported.

1. Introduction

Elastic flow around thin rigid bodies has attracted many researchers due to its relevance to modeling of wedging of brittle bodies and penetration mechanics. The dynamic plane-strain problem of wedging of an elastic plane by a thin semi-infinite rigid body moving at constant sub-Rayleigh speed was analytically solved in (**1**). Ahead of the body a crack was assumed to be formed, and the Coulomb friction law conditions were enforced in the semi-infinite surface of the body. The super-Rayleigh regime model (**2**) assumed the ideal contact conditions ahead of the body, frictionless contact of the body with the medium, and zero traction boundary conditions in the trailing crack. The method of the scalar Riemann-Hilbert problem was employed in (**3**) for solving the plane-strain problem on a thin rigid body moving at transonic constant speed in an elastic infinite medium when a semi-infinite crack trails the body and no friction occurs in the contact surface. Subsonic and transonic steady-state regimes of frictional motion of a finite thin rigid body in an elastic medium with a semi-infinite trailing cavity and without a fore cavity were considered in (**4**, **5**).

During rapid motion of a thin body the elastic medium may separate from the penetrator surface. Different criteria for the determination of the separation point were proposed in the literature. In the model (**1**) the body is semi-infinite, and it is assumed that the medium is not detached from the body. The separation point in the fore part of the body or, equivalently, the initial point of the crack ahead of the body is determined from the boundedness of the normal traction at this point. Different criteria based on the analysis of higher order terms in an asymptotic expansion of the solution were proposed

[†]<yantipov@lsu.edu>

Q. Jl Mech. Appl. Math, Vol. 71. No. 2 © The Author, 2018. Published by Oxford University Press;

Advance Access publication 12 March 2018. doi:10.1093/qjmam/hby003

in (**2**) and (**3**). To find the separation point, the conditions on the normal velocity and acceleration, that is $\partial u_x/\partial x = 0$, $\partial^2 u_x/\partial x^2 = 0$, were enforced in (**4**).

Two-dimensional model problems on rapid motion of thin bodies is also relevant to modeling of penetration of an axisymmetric body into an elastic medium. It is a generally accepted practice in applied mechanics to test and understand a phenomenon on a two-dimensional problem, an analog of the axisymmetric problem, first and then, at the next stage, analyze the three-dimensional problem. The fact that this argument is applicable to penetration mechanics was confirmed by comparison of plane strain and three-dimensional computations (**6**) and experimental results (**7**) when the projectile was modeled as a plate and a rod, respectively.

In this article, we analyze a new model which generalizes the model (**1**) by assuming that the rigid body is finite, not semi-infinite. When the body advances at a sub-Rayleigh speed, two crack-like cavities are formed, a semi-infinite trailing cavity and a finite cavity ahead of the body. In addition, we analyze an analog of this model without the fore cavity. In both models, the separation point, if exists, is identified as the point where the compressive normal traction in the contact area changes its sign and becomes a tensile stress.

In section 2, we formulate the first model which admits the existence of a fore finite crack-like cavity. By employing the theory of analytic functions and the symmetry principle (**4**, **8**, **9**) we reduce the model to two sequently solved by quadratures Riemann-Hilbert problems. We analyze the asymptotic behavior of the normal and tangential traction components and the tangential derivative of the normal displacement (the normal velocity) and show that they are continuous for any choice of the fore and aft separation points. We propose to employ the Griffith criterion for determination of the fore crack length. We derive a new formula for the resistance force that counts not only for the tangential traction component τ_{xy} but also for the stress σ_x (the body is advancing in the x-direction). It is shown that the negligence of the stress σ_x in the formula for the resistance force underestimates its values and leads to the unrealistic zero value of the force as speed reaches the Rayleigh speed. Expanding the solution in terms of the Jacobi polynomials enables us to transform the solution given by singular integrals with the Cauchy kernel to a form convenient for numerical purposes. Numerical results reveal that for all ogive-nose penetrators with a fore cavity analyzed the normal traction is compressive and there is no detachment of the medium from the body.

In section 3, we consider another penetration model when no fore cavity exists. The solution method proposed in section 2 requires only an insignificant modification. Analysis of numerical results shows that in contrast to Model 1 separation of the medium from the body may occur not only in the aft area of the penetrator but also at the fore section. The position of the separation points, if they exist, depends on the body profile and the problem parameters. Numerical results implemented for Models 1 and 2 with and without a fore crack of fixed length reveal that the resistance force decreases with the increase of sub-Rayleigh speed in a fashion similar to the variation of the Mode-I stress intensity factor with speed in dynamic fracture mechanics (**10**). If the crack length varies with speed and the Griffith criterion is employed to determine its length, then the resistance force is not a monotonic function and attains it maximum at a certain sub-Rayleigh speed.

2. Motion of a thin body with a crack-like cavity ahead

2.1 *Formulation*

The model problem to be addressed is the two-dimensional steady-state one presented in Fig. 1. A finite thin rigid body whose surface, at time t, described by

$$S(t) = \{\mathbf{x} : 0 < x_1 - Vt < b,\ x_2 = \pm\omega_0(x_1 - Vt),\ -\infty < x_3 < +\infty\}, \tag{2.1}$$

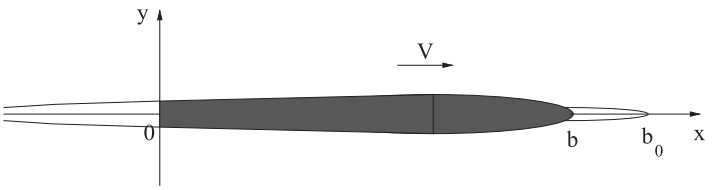

Fig. 1 The geometry of the first model problem when $b_- = 0$ and $b_+ = b$

moves along the plane $\{-\infty < x_1 < +\infty, x_2 = 0, -\infty < x_3 < +\infty\}$. The speed V is constant, $V < c_R$, and c_R is the Rayleigh speed for the elastic medium characterized by the longitudinal and shear waves speeds c_l and c_s, respectively, $c_l = \sqrt{(\lambda + 2\mu)/\rho}$, $c_s = \sqrt{\mu/\rho}$, λ and μ are the Lamé constants, and ρ is the density. The function $\omega_0(x)$ is convex, $b = \text{const}$ all the time, and the conditions of the Coulomb friction law are satisfied in a contact zone $b_- < x_1 - Vt < b_+$, $x_2 = \pm\omega_0(x_1 - Vt)$ between the body and the elastic medium, and $0 \le b_- < b_+ \le b$. These conditions, when linearized, read $\tau_{xy} = \pm k\sigma_y$, $x_2 = 0^{\pm}$, where the normal traction component σ_y is negative on the upper and lower surfaces of the body and $k > 0$ is the dynamic friction coefficient.

It is also assumed that behind the body there is a semi-infinite crack-like cavity, while ahead of the body a finite crack-like cavity $b_+ < x_1 - Vt < b_0$ moves along the plane $x_2 = 0$ at the speed V.

Due to the symmetry the problem it is set in the upper half-plane, and the linearized boundary conditions are written in the line $x_2 = 0$. In the moving coordinates, $x = x_1 - Vt$, $y = x_2$, the boundary conditions are

$$\begin{gathered}\sigma_y = 0, \quad \tau_{xy} = 0, \quad x \in (-\infty, 0) \cup (b_+, b_0),\\ \tau_{xy} = k\sigma_y, \quad u_{y,x} = \omega(x), \quad b_- < x < b_+,\\ \tau_{xy} = 0, \quad u_{y,x} = 0, \quad b_0 < x < +\infty,\end{gathered} \tag{2.2}$$

where $\omega(x) = \omega_0'(x)$. The relations (**10**)

$$\begin{gathered}u_x = \phi_{,x} + \psi_{,y}, \quad u_y = \phi_{,y} - \psi_{,x}, \quad \mu^{-1}\tau_{xy} = 2\phi_{,xy} - \psi_{,xx} + \psi_{,yy},\\ \mu^{-1}\sigma_x = c\phi_{,xx} + (c-2)\phi_{,yy} + 2\psi_{,xy}, \quad \mu^{-1}\sigma_y = (c-2)\phi_{,xx} + c\phi_{,yy} - 2\psi_{,xy}\end{gathered} \tag{2.3}$$

represent the displacements and the stress tensor components in terms of the derivatives of the displacement potentials $\phi(x, y)$ and $\psi(x, y)$. Here, $c = c_l^2/c_s^2$. The functions ϕ and ψ solve the wave equations which, in the moving coordinates (x, y), read (**10**)

$$\alpha_l^2\phi_{,xx} + \phi_{,yy} = 0, \quad \alpha_s^2\psi_{,xx} + \psi_{,yy} = 0, \quad -\infty < x < +\infty, \quad 0 < y < +\infty, \tag{2.4}$$

where

$$\alpha_l = \sqrt{1 - \frac{V^2}{c_l^2}}, \quad \alpha_s = \sqrt{1 - \frac{V^2}{c_s^2}}. \tag{2.5}$$

2.2 *Two symmetric Riemann–Hilbert problems and their solution*

Let $\phi(x, y) = \operatorname{Re}\Phi(z_l)$ and $\psi(x, y) = \operatorname{Re}\Psi(z_s)$, where $z_l = x + i\alpha_l y$, $z_s = x + i\alpha_s y$, and $\Phi(z)$ and $\Psi(z)$ are analytic functions in the complex plane cut along the line $-\infty < \operatorname{Re} z < b_2$, $\operatorname{Im} z = 0$. Then (2.4) are automatically satisfied. The stress components and the normal displacement derivative needed are given by (**10**)

$$\begin{aligned}
\mu^{-1}\sigma_x &= (1 - \alpha_s^2 + 2\alpha_l^2)\operatorname{Re}\Phi''(z_l) - 2\alpha_s \operatorname{Im}\Psi''(z_s),\\
\mu^{-1}\sigma_y &= -(1 + \alpha_s^2)\operatorname{Re}\Phi''(z_l) + 2\alpha_s \operatorname{Im}\Psi''(z_s),\\
\mu^{-1}\tau_{xy} &= -2\alpha_l \operatorname{Im}\Phi''(z_l) - (1 + \alpha_s^2)\operatorname{Re}\Psi''(z_s),\\
u_{y,x} &= -\alpha_l \operatorname{Im}\Phi''(z_l) - \operatorname{Re}\Psi''(z_s).
\end{aligned} \tag{2.6}$$

Note that the function $-Vu_{y,x}$ can also be interpreted as the normal component of the velocity vector, $\dot{u}_y = -Vu_{y,x}$. Due to the relations (2.6) for the stresses σ_y and τ_{xy} to simplify the boundary conditions, it will be convenient to deal with two new functions analytic in the upper half-plane. They are

$$\begin{aligned}
\Omega_1(z) &= -(1 + \alpha_s^2)\Phi''(z) - 2i\alpha_s\Psi''(z),\\
\Omega_2(z) &= 2\alpha_l\Phi''(z) + i(1 + \alpha_s^2)\Psi''(z).
\end{aligned} \tag{2.7}$$

On inverting these relations, we connect the real and imaginary parts of the original and new functions as

$$\begin{aligned}
\operatorname{Re}\Phi''(z_l) &= \frac{1 + \alpha_s^2}{R}\operatorname{Re}\Omega_1(z_l) + \frac{2\alpha_s}{R}\operatorname{Re}\Omega_2(z_l),\\
\operatorname{Im}\Phi''(z_l) &= \frac{1 + \alpha_s^2}{R}\operatorname{Im}\Omega_1(z_l) + \frac{2\alpha_s}{R}\operatorname{Im}\Omega_2(z_l),\\
\operatorname{Re}\Psi''(z_s) &= -\frac{2\alpha_l}{R}\operatorname{Im}\Omega_1(z_s) - \frac{1 + \alpha_s^2}{R}\operatorname{Im}\Omega_2(z_s),\\
\operatorname{Im}\Psi''(z_s) &= \frac{2\alpha_l}{R}\operatorname{Re}\Omega_1(z_s) + \frac{1 + \alpha_s^2}{R}\operatorname{Re}\Omega_2(z_s).
\end{aligned} \tag{2.8}$$

Here,

$$R = 4\alpha_s\alpha_l - (1 + \alpha_s^2)^2 > 0. \tag{2.9}$$

We next substitute these formulas into (2.6) to obtain

$$\begin{aligned}
\mu^{-1}R\sigma_x &= [(1 + \alpha_l^2)^2 - (\alpha_l^2 - \alpha_s^2)^2 - 4\alpha_l\alpha_s]\operatorname{Re}\Omega_1(x) + 4\alpha_s(\alpha_l^2 - \alpha_s^2)\operatorname{Re}\Omega_2(x),\\
\mu^{-1}\sigma_y &= \operatorname{Re}\Omega_1(x), \quad \mu^{-1}\tau_{xy} = -\operatorname{Im}\Omega_2(x),\\
Ru_{y,x} &= q\operatorname{Im}\Omega_1(x) + k^{-1}p\operatorname{Im}\Omega_2(x),
\end{aligned} \tag{2.10}$$

where p and q are two positive parameters given by

$$p = k(1 - 2\alpha_s\alpha_l + \alpha_s^2), \quad q = \alpha_l(1 - \alpha_s^2). \tag{2.11}$$

The boundary conditions (2.2) in terms of the new functions Ω_1 and Ω_2 take the form

$$\begin{gathered}\operatorname{Re}\Omega_1(x)=0,\quad \operatorname{Im}\Omega_2(x)=0,\quad -\infty<x<b_-,\quad b_+<x<b_0,\\ k\operatorname{Re}\Omega_1(x)+\operatorname{Im}\Omega_2(x)=0,\quad q\operatorname{Im}\Omega_1(x)+k^{-1}p\operatorname{Im}\Omega_2(x)=R\omega(x),\quad b_-<x<b_+,\\ \operatorname{Im}\Omega_1(x)=0,\quad \operatorname{Im}\Omega_2(x)=0,\quad b_0<x<+\infty.\end{gathered}\tag{2.12}$$

On aiming to reduce this problem to a vector Riemann–Hilbert problem we extend the definition of the functions $\Omega_j(z)$ to the lower half-plane. Denote

$$\Omega_j^+(z)=\Omega_j(z),\quad \Omega_j^-(z)=\overline{\Omega_j^+(\bar z)},\quad j=1,2.\tag{2.13}$$

Then the functions $\Omega_1^\pm(z)$ and $\Omega_2^\pm(z)$ are defined and analytic in the half-planes $C^\pm=\{\pm\operatorname{Re}z>0\}$. This expansion and the boundary conditions (2.12) enable us to reformulate the problem as the following two symmetric Riemann–Hilbert problem to be solved sequently.

Find piece-wise analytic functions $\Omega_1(z)$ and $\Omega_2(z)$, Hölder continuous up to the real axis, satisfying the symmetry condition (2.13) in the plane and whose limiting values $\Omega_j(x\pm i0)=\Omega_j^\pm(x)$ meet the boundary conditions

$$\Omega_1^+(x)=G(x)\Omega_1^-(x)+g_1(x),\quad -\infty<x<+\infty,\tag{2.14}$$

and

$$\Omega_2^+(x)=\Omega_2^-(x)+g_2(x),\quad -\infty<x<+\infty.\tag{2.15}$$

Here,

$$G(x)=\begin{cases}-(p-iq)/(p+iq), & b_-<x<b_+,\\ -1, & -\infty<x<b_-,\ b_+<x<b_0,\\ 1, & b_0<x<+\infty,\end{cases}$$

$$g_1(x)=\begin{cases}-2R\omega(x)/(p+iq), & b_-<x<b_+,\\ 0, & x\notin[b_-,b_+],\end{cases}\quad g_2(x)=\begin{cases}-2ki\operatorname{Re}\Omega_1(x), & b_-<x<b_+,\\ 0, & x\notin[b_-,b_+].\end{cases}\tag{2.16}$$

To solve the first problem, we symmetrically factorize the function $G(x)$,

$$G(x)=X^+(x)[X^-(x)]^{-1},\quad -\infty<x<+\infty,\quad X^+(z)=\overline{X^-(\bar z)},\quad z\in C^+.\tag{2.17}$$

This can be done by means of the function

$$\begin{aligned}X(z)&=(z-b_0)^{-1/2}(z-b_+)\exp\left\{\frac{1}{2\pi i}\int_{b_-}^{b_+}\frac{\log[(p-iq)/(p+iq)]d\xi}{\xi-z}\right\}\\ &=(z-b_-)^{\kappa}(z-b_+)^{1-\kappa}(z-b_0)^{-1/2},\end{aligned}\tag{2.18}$$

where

$$\kappa=\frac{1}{\pi}\tan\frac{q}{p}\in\left(0,\frac{1}{2}\right),\tag{2.19}$$

and the branches of the power functions are defined in the plane cut along the ray $-\infty < x < b_0$. They are fixed by the conditions

$$-\pi < \arg(z - b_\pm) < \pi, \quad -\pi < \arg(z - b_0) < \pi. \tag{2.20}$$

This choice of the branches guarantees that the symmetry condition (2.17) is met. To verify that the functions $X^+(x)$ and $X^-(x)$ provide a solution to the factorization problem (2.17), we note that

$$\begin{aligned}(z - b_0)^{-1/2} &= \mp i|x - b_0|^{-1/2}, \quad z = x \pm i0, \quad x < b_0,\\ (z - b_+)^{1-\kappa} &= -e^{\mp\pi i\kappa}|x - b_+|^{1-\kappa}, \quad z = x \pm i0, \quad x < b_+,\\ (z - b_-)^{\kappa} &= e^{\pm\pi i\kappa}|x - b_-|^{\kappa}, \quad z = x \pm i0, \quad x < b_-.\end{aligned} \tag{2.21}$$

The functions $(z - b_0)^{-1/2}$, $(z - b_+)^{1-\kappa}$, and $(z - b_-)^{\kappa}$ are real and positive when $z = x$ and $x > b_0$, $x > b_+$, and $x > b_-$, respectively. This and the relations (2.20) and (2.21) imply that $X^+(z) = \overline{X^-(-z)}$ and also

$$\begin{gathered}X^+(x) = -X^-(x), \quad x \in (-\infty, b_-) \cup (b_+, b_0), \quad X^+(x) = X^-(x), \quad x \in (b_0, +\infty),\\ \frac{X^+(x)}{X^-(x)} = -e^{-2\pi i\kappa} = -\frac{p - iq}{p + iq}, \quad x \in (b_-, b_+).\end{gathered} \tag{2.22}$$

We remark that the factorization function (2.18) is not unique: the function

$$X(z) = (z - b_-)^{\kappa+n_-}(z - b_+)^{1-\kappa+n_+}(z - b_0)^{-1/2+n_0} \tag{2.23}$$

is also a solution to the problem (2.17) provided the numbers $n_\pm$ and n_0 are integers. It turns out that the choice $n_- = n_+ = n_0 = 0$ is the most convenient for the next step of the procedure when it is required to write down the solution to the Riemann–Hilbert problem (2.14) in the class of functions admitting integrable singularity at the point $x = b_0$ and bounded at the points b_- and b_+.

Introduce next the Cauchy integral

$$\Lambda(z) = -\frac{2R}{p + iq}\frac{1}{2\pi i}\int_{b_-}^{b_+}\frac{\omega(\xi)d\xi}{X^+(\xi)(\xi - z)}. \tag{2.24}$$

By substituting the factorization (2.17) and the Sokhotski–Plemelj formula for the limiting values $\Lambda^\pm(x) = \Lambda(x \pm i0)$,

$$\Lambda^+(x) - \Lambda^-(x) = -\frac{2R\omega(x)}{(p + iq)X^+(x)}, \tag{2.25}$$

into the boundary condition (2.14), applying the continuity principle and the Liouville theorem we eventually arrive at the solution of the first Riemann–Hilbert problem

$$\begin{gathered}\Omega_1(z) = X(z)\Lambda(z), \quad z \in C^+,\\ \Omega_1^+(x) = -\frac{R}{p + iq}\left[\omega(x)\chi(x; b_-, b_+) + \frac{X^+(x)}{\pi i}\int_{b_-}^{b_+}\frac{\omega(\xi)d\xi}{X^+(\xi)(\xi - x)}\right], \quad -\infty < x < +\infty,\end{gathered} \tag{2.26}$$

where $\chi(x; b_-, b_+) = 1$ if $x \in [b_-, b_+]$ and 0 otherwise. The solution found has the square root singularity as $z \to b_0$, is bounded at the points $x = b_-$ and $x = b_+$ and decay at infinity as const $z^{-1/2}$.

To write down the solution of the second Riemann–Hilbert problem, one needs to find $\operatorname{Re}\Omega_1^+(x)$, $x \in (b_-, b_+)$. It is given by

$$\operatorname{Re}\Omega_1^+(x) = -\frac{R}{p^2+q^2}\left[p\omega(x) - \frac{qX^+(x)}{\pi}\int_{b_-}^{b_+}\frac{\omega(\xi)d\xi}{X^+(\xi)(\xi-x)}\right], \quad b_- < x < b_+. \tag{2.27}$$

The function $\Omega_2(z)$ is expressed as the Cauchy integral with this density

$$\Omega_2(z) = -\frac{k}{\pi}\int_{b_-}^{b_+}\frac{\operatorname{Re}\Omega_1^+(\xi)d\xi}{\xi - z}. \tag{2.28}$$

Its limiting value $\Omega_2^+(x)$ is

$$\Omega_2^+(x) = -ki\operatorname{Re}\Omega_1^+(x)\chi(x; b_-, b_+) - \frac{k}{\pi}\int_{b_-}^{b_+}\frac{\operatorname{Re}\Omega_1^+(\xi)d\xi}{\xi - x}, \quad -\infty < x < +\infty. \tag{2.29}$$

It can be easily checked that the solution derived satisfies the symmetry condition $\Omega_j^-(z) = \overline{\Omega_j^+(\bar{z})}$, $z \in C^+$, and by the Sokhotski–Plemelj formulas, $\Omega_j^-(x) = \overline{\Omega_j^+(x)}$, $-\infty < x < +\infty$, $j = 1, 2$.

2.3 *Analysis of the solution. Stresses and the normal displacement*

It is now of interest to derive expressions for the traction components and the normal velocity $V_y = -Vu_{y,x}$ and analyze them at the singular points $x = b_-$, b_+, b_0, and ∞. We start with the function $u_{y,x}$. Due to the choice (2.20) of the branches of the factors of the function $X^+(x)$ we have

$$\frac{X^+(x)}{X^+(\xi)} = e^{i\pi\kappa}\left|\frac{X^+(x)}{X^+(\xi)}\right|, \quad -\infty < x < b_-, \quad b_- < \xi < b_+, \tag{2.30}$$

and therefore

$$\Omega_1^+(x) = \frac{R(ip+q)e^{i\pi\kappa}}{\pi(p^2+q^2)}\int_{b_-}^{b_+}\left|\frac{X^+(x)}{X^+(\xi)}\right|\frac{\omega(\xi)d\xi}{\xi - x}, \quad -\infty < x < b_-, \tag{2.31}$$

Taking the imaginary part of this function and since $\operatorname{Im}\Omega_2^+(x) = 0$, we obtain

$$u_{y,x} = -V^{-1}V_y = \frac{\sin\pi\kappa}{\pi}\int_{b_-}^{b_+}\left|\frac{X^+(x)}{X^+(\xi)}\right|\frac{\omega(\xi)d\xi}{\xi - x}, \quad -\infty < x < b_-. \tag{2.32}$$

Similarly,

$$u_{y,x} = -V^{-1}V_y = -\frac{\sin\pi\kappa}{\pi}\int_{b_-}^{b_+}\left|\frac{X^+(x)}{X^+(\xi)}\right|\frac{\omega(\xi)d\xi}{\xi - x}, \quad b_+ < x < b_0. \tag{2.33}$$

It is directly verified that $u_{y,x} = \omega(x)$ if $b_- < x < b_+$ and $u_{y,x} = 0$ if $x > b_0$.

Analyze next the behavior of the function $u_{y,x}(x,0)$ as $x \to b_-$ and $x \to b_+$. At the endpoints $b_\pm$, the Cauchy integral whose density has a power singularity behaves as (**11**)

$$\frac{1}{2\pi i}\int_{b_-}^{b_+}\frac{d\xi}{(\xi-b_\pm)^\gamma(\xi-x)} = \mp\frac{e^{\mp i\pi\gamma}}{2i\sin\pi\gamma}(x-b_\pm)^{-\gamma} + M_\pm(x), \quad x \to b_\pm \pm 0, \tag{2.34}$$

where $M_\pm(z)$ are functions analytic at the points $b_\pm$, respectively. On employing this formula and also (2.20) we obtain for the function $\Omega_1^+(x)$

$$\Omega_1^+(x) \sim \frac{iR(p-iq)e^{i\pi\kappa}}{(p^2+q^2)\sin\pi\kappa}\omega(b_\pm), \quad x \to b_\pm \pm 0. \tag{2.35}$$

Since $\tan\pi\kappa = q/p$, we deduce $\operatorname{Im}\Omega_1^+(x) \sim q^{-1}R\omega(b_\pm)$, $x \to b_\pm \pm 0$. Therefore

$$u_{y,x}(x,0) = -V^{-1}V_y = \omega(b_\pm), \quad x \to b_\pm \pm 0. \tag{2.36}$$

We thus have shown that at the point $x = b_-$ and $x = b_=$ the normal velocity is continuous and the profiles of the cavities are smooth regardless of the choice of the points $b_\pm$.

Prove next that the traction components σ_y and τ_{xy} vanish at the points $x = b_\pm$ and therefore are continuous. In the interval (b_-, b_+), $\sigma_y(x,0) = \mu\operatorname{Re}\Omega_1^+(x)$, and the function $\operatorname{Re}\Omega_1^+(x)$ is given by (2.27). The principal value of the Cauchy integral whose density has a power singularity at the endpoints admits the representation (**11**)

$$\frac{1}{2\pi i}\int_{b_-}^{b_+}\frac{d\xi}{(\xi-b_\pm)^\gamma(\xi-x)} = \mp\frac{\cot\pi\gamma}{2i}(x-b_\pm)^{-\gamma} + M_\pm(x), \quad x \to b_\pm \mp 0. \tag{2.37}$$

This enables us to obtain

$$\sigma_y = \mu\operatorname{Re}\Omega_1(x) \sim -\frac{\mu R}{p^2+q^2}(p - q\cot\pi\kappa) = 0, \quad x \to b_\pm \mp 0. \tag{2.38}$$

Due to the boundary condition (2.2) the tangential traction component vanishes at the points $b_\pm$ as well, $\tau_{xy} = k\sigma_y \sim 0$, $x \to b_\pm \mp 0$.

It is seen that, in general, as $x \to -\infty$, the function $u_{y,x}(x,0) \sim \omega_*(-x)^{-1/2}$, where

$$\omega_* = \frac{\sin\pi\kappa}{\pi}\int_{b_-}^{b_+}\frac{\sqrt{b_0-\xi}\,\omega(\xi)d\xi}{(\xi-b_-)^\kappa(b_+-\xi)^{1-\kappa}}. \tag{2.39}$$

If $\omega(x) < 0$ for all $x \in (0,b)$, then $\omega_* \neq 0$ regardless of the choice of the parameters b_- and b_+. If however the function $\omega(x)$ changes its sign in the interval $(0,b)$, that is if the profile function $\omega_0(x)$ attains its local maximum at a point $b_* \in (0,b)$, then the parameter ω_* may become zero for a certain location of the point b_- and then $u_{y,x}(x,0) = O(|x|^{-3/2})$ as $x \to -\infty$. The points b_- and b_+ have to be selected such that the traction component σ_y is negative everywhere in the interval (b_-, b_+), and b_- and b_+ are the nearest points to $x = 0$ and $x = b$, respectively.

It is directly verified from the formulas for $\sigma_y(x,0) = \mu\operatorname{Re}\Omega_1(x)$ and $\tau_{xy}(x,0) = -\mu\operatorname{Im}\Omega_2(x)$ that $\sigma_y(x,0) = 0$ when $x \le b_-$ and $b_- \le x < b_0$, while $\tau_{x,y} = 0$ if $x \le b_-$ and $b_+ \le x < +\infty$.

In the semi-infinite segment $(b_0, +\infty)$, the stress $\sigma_y(x, 0) = \mu \operatorname{Re} \Omega_1^+(x)$, and it does not vanish. We have

$$\sigma_y(x.0) = -\frac{\mu R \sin \pi\kappa}{\pi q} \frac{(x - b_-)^\kappa (x - b_+)^{1-\kappa}}{\sqrt{x - b_0}} \int_{b_-}^{b_+} \frac{\sqrt{b_0 - \xi}\omega(\xi)d\xi}{(\xi - b_-)^\kappa (b_+ - \xi)^{1-\kappa}(x - \xi)}, \quad x > b_0. \tag{2.40}$$

Therefore the stress $\sigma_y(x, 0)$ has the square root singularity as $x \to b_0 + 0$,

$$\sigma_y(x, 0) \sim \frac{K_I}{\sqrt{2\pi}}(x - b_0)^{-1/2}, \quad x \to b_0 + 0, \tag{2.41}$$

where K_I is the stress singularity factor (SIF)

$$K_I = -\frac{\sqrt{2}\mu R \sin \pi\kappa (b_0 - b_-)^\kappa (b_0 - b_+)^{1-\kappa}}{\sqrt{\pi} q} \int_{b_-}^{b_+} \frac{\omega(\xi)d\xi}{(\xi - b_-)^\kappa (b_+ - \xi)^{1-\kappa}\sqrt{b_0 - \xi}}. \tag{2.42}$$

2.4 *Definition of the parameter b_0 and the resistance force*

The potential energy δU released when the cavity ahead of the body, $C(t) = \{b_+ < x_1 - Vt < b_0, x_2 = 0\}$ extends to $C(t) + \delta C(t) = \{b_+ + r < x_1 - Vt < b_0 + r, x_2 = 0\}$, r is small, is

$$\delta U = \frac{1}{2} \int_{b_0}^{b_0 + r} \sigma_y(x, 0)\delta[u_y](x)dx. \tag{2.43}$$

Here, $[u_y] + \delta[u_y]$ is the displacement jump related to the extended cavity. From formula (2.33) for the extended cavity due to the symmetry we have

$$\delta[u_{y,x}] \sim \frac{2 \sin \pi\kappa (b_0 - b_-)^\kappa (b_0 - b_+)^{1-\kappa}}{\pi\sqrt{r + b_0 - x}} \int_{b_-}^{b_+} \frac{\omega(\xi)d\xi}{(\xi - b_-)^\kappa (b_+ - \xi)^{1-\kappa}\sqrt{b_0 - \xi}}. \; x \to b_0 + r - 0. \tag{2.44}$$

This can be rewritten in terms of the SIF K_I given by (2.42) as

$$\delta[u_{y,x}] \sim -\frac{\sqrt{2}qK_I}{\sqrt{\pi}\mu R}(b_0 + r - x)^{-1/2}, \quad x \to b_0 + r - 0. \tag{2.45}$$

On integrating the last relation we derive

$$\delta[u_y] \sim 2\sqrt{\frac{2}{\pi}} \frac{a_l V^2 K_I}{c_s^2 \mu R} \sqrt{b_0 + r - x}, \quad x \to b_0 + r - 0. \tag{2.46}$$

Substitution of the relations (2.41) and (2.46) into (2.43) leads to

$$\delta U \sim \frac{rV^2 a_l K_I^2}{2\mu c_s^2 R}. \tag{2.47}$$

Notice that this expression is consistent with the expression for the increment of the potential energy when a Mode-I crack is growing (**10**, **12**). According to the Griffith criterion, the crack

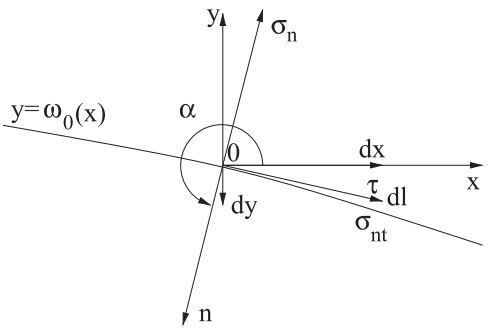

Fig. 2 The traction components σ_n and σ_{nt} acting on the body surface

starts propagating if the potential energy $\delta U(t)$ equals or greater than the increase in the surface energy $2Tr$, that is $\delta U \geq 2Tr$, where T is the Griffith material constant. Equivalently, this criterion can be written as

$$K_I^2 \geq \frac{4Tc_s^2\mu R}{V^2 a_l}. \tag{2.48}$$

On applying this criterion we derive a transcendental equation for the cavity length b_0. It has the form

$$\frac{\sin \pi\kappa (b_0 - b_-)^\kappa}{q(b_0 - b_+)^{\kappa-1}} \int_{b_-}^{b_+} \frac{(b_+ - \xi)^{\kappa-1}\omega(\xi)d\xi}{(\xi - b_-)^\kappa \sqrt{b_0 - \xi}} + \frac{c_s}{V}\sqrt{\frac{2\pi T}{a_l \mu R}} = 0. \tag{2.49}$$

The magnitude of the resistance force due to the motion of the body is defined by

$$F = 2\int_{b_-b_+} \left\{[-\sigma_n|_{y=\omega_0}]_x + [\sigma_{nt}|_{y=\omega_0}]_x\right\} dl. \tag{2.50}$$

Here, b_-b_+ is the portion of the upper surface contacting with the elastic medium, dl is the elementary arc length, $\sigma_n|_{y=\omega_0}$ and $\sigma_{nt}|_{y=\omega_0}$ are the traction components with the normal n to the surface $y = \omega(x)$ directed inside the penetrator (Fig. 2), and $[\sigma_n|_{y=\omega_0}]_x$ and $[\sigma_{nt}|_{y=\omega_0}]_x$ are their projections on the x-axis. To express the integrand in the integral (2.50) through the stresses σ_x, σ_y, and τ_{xy}, we write

$$\begin{aligned} \sigma_n &= \cos^2\alpha\,\sigma_x + \sin^2\alpha\,\sigma_y + \sin 2\alpha\,\tau_{xy}, \\ \sigma_{nt} &= \frac{1}{2}\sin 2\alpha\,(\sigma_y - \sigma_x) + \cos 2\alpha\,\tau_{xy}, \end{aligned} \tag{2.51}$$

where α is the angle between the x-axis and the normal n, $\pi \leq \alpha \leq \frac{3}{2}\pi$. Notice, that for approximately flat surfaces parallel to the plane $y = 0$, $\alpha \approx \frac{3\pi}{2}$ and $\sigma_n \approx \sigma_y < 0$, while $\sigma_{nt} \approx -\tau_{xy} > 0$. Now, since $dy = \omega dx$ and

$$\begin{aligned} [-\sigma_n|_{y=\omega_0}]_x &= \sigma_n \cos\alpha = \omega\sigma_n \frac{dx}{dl}, \\ [\sigma_{nt}|_{y=\omega_0}]_x &= -\sigma_{nt}\sin\alpha = \sigma_{nt}\frac{dx}{dl}, \end{aligned} \tag{2.52}$$

we express the integral F as

$$F = 2\int_{b_-}^{b_+} (\omega\sigma_n + \sigma_{nt})dx. \tag{2.53}$$

For $\alpha = \frac{3\pi}{2} - \varepsilon$ with ε being small, $\omega < 0$, $\sigma_n < 0$, $\sigma_{nt} > 0$, and $F > 0$. Using next the relations (2.51), the trigonometric identities

$$\begin{aligned} \sin^2\alpha &= \frac{1}{1+\omega^2}, \quad \cos^2\alpha = \frac{\omega^2}{1+\omega^2}, \\ \cos 2\alpha &= -\frac{1-\omega^2}{1+\omega^2}, \quad \sin 2\alpha = -\frac{2\omega}{1+\omega^2}, \end{aligned} \tag{2.54}$$

and since $\tau_{xy} = k\sigma_y$, we have

$$F = 2\int_{b_-}^{b_+} (\omega\sigma_x - \tau_{xy})dx. \tag{2.55}$$

Here,

$$\begin{aligned} \sigma_x &= \frac{\mu}{R}\{[(1+\alpha_l^2)^2 - (\alpha_l^2 - \alpha_s^2)^2 - 4\alpha_l\alpha_s]\,\mathrm{Re}\,\Omega_1^+(x) + 4\alpha_s(\alpha_l^2 - \alpha_s^2)\,\mathrm{Re}\,\Omega_2^+(x)\}, \\ \tau_{xy} &= \mu k\,\mathrm{Re}\,\Omega_1^+(x). \end{aligned} \tag{2.56}$$

$\mathrm{Re}\,\Omega_1^+(x)$ is given by (2.27) and from (2.29)

$$\mathrm{Re}\,\Omega_2^+(x) = -\frac{k}{\pi}\int_{b_-}^{b_+} \frac{\mathrm{Re}\,\Omega_1^+(\xi)d\xi}{\xi - x}. \tag{2.57}$$

2.5 *Computational formulas*

First we transform formula (2.27) for the normal traction component $\sigma_y = \mu\,\mathrm{Re}\,\Omega_1^+(x)$ to a form convenient for computations. To do this we write

$$\sigma_y(x,0) = -\frac{\mu R}{p^2+q^2}\left[p\omega(x) - \frac{q(x-b_-)^\kappa(b_+-x)^{1-\kappa}}{\pi\sqrt{b_0-x}}I(x)\right], \quad b_- < x < b_+, \tag{2.58}$$

where

$$I(x) = \int_{b_-}^{b_+} \frac{\sqrt{b_0-\xi}\,\omega(\xi)d\xi}{(\xi-b_-)^\kappa(b_+-\xi)^{1-\kappa}(\xi-x)}. \tag{2.59}$$

To compute the principal value of this Cauchy integral we change the variables and notations

$$\begin{aligned} \xi &= (b_+ - b_-)\tau + b_-, \quad x = (b_+ - b_-)t + b_-, \\ f(\tau) &= \sqrt{b_0 - b_- - (b_+ - b_-)\tau}\,\omega((b_+ - b_-)\tau + b_-) \end{aligned} \tag{2.60}$$

to derive

$$I(x) = \frac{1}{b_+ - b_-} \int_0^1 \frac{f(\tau) d\tau}{\tau^\kappa (1-\tau)^{1-\kappa} (\tau - t)}. \tag{2.61}$$

On expanding the function $f(\tau)$ in terms of the Jacobi polynomials $P_n^{-\kappa,\kappa-1}(1-2\tau)$

$$f(\tau) = \sum_{n=0}^{\infty} f_n P_n^{-\kappa,\kappa-1}(1-2\tau) \tag{2.62}$$

and using the relation (**13**)

$$\int_0^1 \tau^{-\kappa}(1-\tau)^{\kappa-1} P_n^{-\kappa,\kappa-1}(1-2\tau) \frac{d\tau}{\tau - t}$$
$$= \pi \cot \pi\kappa\, t^{-\kappa}(1-t)^{\kappa-1} P_n^{-\kappa,\kappa-1}(1-2t) - \frac{\pi}{\sin \pi\kappa} P_{n-1}^{\kappa,1-\kappa}(1-2t), \quad 0 < t < 1, \tag{2.63}$$

we find a series representation of the integral $I(x)$

$$I(x) = \pi \sum_{n=0}^{\infty} f_n \left[\frac{\cot \pi\kappa (b_+ - x)^{\kappa-1}}{(x-b_-)^\kappa} P_n^{-\kappa,\kappa-1}\left(\frac{b^+ - x}{b^-}\right) - \frac{\csc \pi\kappa}{b_+ - b_-} P_{n-1}^{\kappa,1-\kappa}\left(\frac{b^+ - x}{b^-}\right)\right]. \tag{2.64}$$

Here, $b^\pm = \frac{1}{2}(b_+ \pm b_-)$ and $P_{n-1}^{\kappa,1-\kappa}(\cdot) = 0$ if $n = 0$. Now, if we recall that $\cot \pi\kappa = p/q$ and that

$$\sum_{n=0}^{\infty} f_n P_n^{-\kappa,\kappa-1}\left(\frac{b^+ - x}{b^-}\right) = \sqrt{b_0 - x}\,\omega(x), \tag{2.65}$$

we discover from (2.58)

$$\sigma_y(x,0) = -\frac{\mu R \sin \pi\kappa (x-b_-)^\kappa (b_+ - x)^{1-\kappa}}{q(b_+ - b_-)\sqrt{b_0 - x}} \sum_{n=1}^{\infty} f_n P_{n-1}^{\kappa,1-\kappa}\left(\frac{b^+ - x}{b^-}\right), \quad b_- < x < b_+. \tag{2.66}$$

The expansion coefficients f_n are recovered from (2.62) as

$$f_n = \frac{1}{\lambda_n^2} \int_0^1 f(\tau) \tau^{-\kappa}(1-\tau)^{\kappa-1} P_n^{-\kappa,\kappa-1}(1-2\tau) d\tau, \tag{2.67}$$

where

$$\lambda_n^2 = \frac{\pi (\kappa)_n (1-\kappa)_n}{2n!^2 \sin \pi\kappa}, \tag{2.68}$$

and $(a)_n = a(a+1)\dots(a+n-1)$ is the factorial symbol. The integrand in (2.67) has power singularities at the ends. It can can be expressed through the following two regular integrals:

$$f_n = \frac{1}{\lambda_n^2}(I_n^0 + I_n^1), \tag{2.69}$$

where

$$I_n^0 = \int_0^{1/2} \left[f(\tau)(1-\tau)^{\kappa-1} P_n^{-\kappa,\kappa-1}(1-2\tau) - \frac{f(0)(1-\kappa)_n}{n!} \right] \tau^{-\kappa} d\tau + \frac{f(0)(2-\kappa)_{n-1}}{2^{1-\kappa} n!},$$

$$I_n^1 = \int_{1/2}^1 \left[f(\tau)\tau^{-\kappa} P_n^{-\kappa,\kappa-1}(1-2\tau) - \frac{f(1)(\kappa)_n}{(-1)^n n!} \right] (1-\tau)^{\kappa-1} d\tau + \frac{f(1)(\kappa+1)_{n-1}}{(-1)^n 2^\kappa n!}. \quad (2.70)$$

This transformation enables us to evaluate the integrals by using the Simpson integration rule.

In the segment $b_- < x < b_+$, the stress $\sigma_x(x, 0)$ is expressed through $\operatorname{Re}\Omega_1^+(x) = \mu^{-1}\sigma_y$ and $\operatorname{Re}\Omega_2^+(x)$ is given by formula (2.56). Due to formula (2.66) the function $\operatorname{Re}\Omega_1^+(\xi)$ tends to zero at the endpoints, and computation of the Cauchy integral (2.29) can be done in the following simple way:

$$\operatorname{Re}\Omega_2^+(x) = -\frac{k}{\pi} \int_{b_-}^{b_+} \frac{[\operatorname{Re}\Omega_1^+(\xi) - \operatorname{Re}\Omega_1^+(x)]d\xi}{\xi - x} - \frac{k}{\pi} \operatorname{Re}\Omega_1^+(x) \log \frac{b_+ - x}{x - b_-}. \quad (2.71)$$

To compute the SIF K_I given by the integral (2.42), we notice that the integrand has power singularities of orders $\kappa \in (0, \frac{1}{2})$ and $1-\kappa \in (\frac{1}{2}, 1)$ at the endpoints $\xi = b_-$ and $\xi = b_+$, respectively. For computations, it is convenient to rewrite formula (2.42) as

$$K_I = -K_0 \left[\frac{\pi\omega(b_+)}{\sqrt{b_0 - b_+}\sin\pi\kappa} + J \right], \quad (2.72)$$

where

$$K_0 = \sqrt{\frac{2}{\pi}} \frac{\mu R \sin\pi\kappa}{q} (b_0 - b_-)^\kappa (b_0 - b_+)^{1-\kappa},$$

$$J = \int_{b_-}^{b_+} \frac{\omega(\xi)(b_0 - \xi)^{-1/2} - \omega(b_+)(b_0 - b_+)^{-1/2}}{(\xi - b_-)^\kappa (b_+ - \xi)^{1-\kappa}} d\xi. \quad (2.73)$$

The integral J was evaluated numerically by the order-N Gauss quadrature formula

$$J = \int_{-1}^1 \frac{g^\circ(\tau)d\tau}{\sqrt{1-\tau^2}} = \frac{\pi}{N} \sum_{j=1}^N g^\circ(x_j), \quad x_j = \cos\frac{(2j-1)\pi}{2N}, \quad (2.74)$$

where

$$g^\circ(\tau) = (1+\tau)^{1/2-\kappa}(1-\tau)^{\kappa-1/2} \left[\omega(b^-\tau + b^+)(b_0 - b^-\tau - b^+)^{-1/2} - \frac{\omega(b_+)}{\sqrt{b_0 - b_+}} \right] \quad (2.75)$$

and $g^\circ(\tau) = O((1-\tau)^{\kappa+1/2})$, $\tau \to 1$.

2.6 *Numerical results*

Computational tests were implemented for the SIF, the stresses σ_x and σ_y on the contact surface $y = \omega_0(x)$ between the elastic medium and the rigid body, and the resistance force due to the stresses σ_x and τ_{xy}.

To describe the upper profile of the fore part of the body, $y = \omega_0(x) \in [0, h]$, $x \in [\gamma_0, b]$, consider an ellipse $\alpha_0^{-2}(x - x_0)^2 + \beta_0^{-2}(y - y_0)^2 = 1$ with $\beta_0 < \alpha_0 < b$, $\beta_0 > h$, $2\alpha_0 < b$, and with the center (x_0, y_0) lying bellow the x-axis. Select a point (x_2, y_2) in the upper part of the ellipse with $x_2 \in [x_0, b)$. Assume that the fore part of the upper part of the body is described by the arc of ellipse with $x_2 \le x \le b$, $0 \le y \le h$. Consider three profiles. In the first case $x_0 < x_2 < b$, and the upper profile consists of the fore elliptic part and the straight part $y = d(x - x_2) + y_2$, $0 \le x \le x_2$ with the parameter d chosen such $y'(x_2 - 0) = y'(x_2 + 0)$. Although the parameter x_2 is free, it has to be chosen such that the point (x_2, y_2) is close to the ellipse vertex (x_0, h) to avoid large slopes of the straight segment of the profile. The parameters y_2 and d are expressed through the other parameters as

$$y_2 = y_0 + \beta_0\sqrt{1 - \left(\frac{x_2 - x_0}{\alpha_0}\right)^2}, \quad d = -\frac{\beta_0(x_2 - x_0)}{\alpha_0^2}\left[1 - \left(\frac{x_2 - x_0}{\alpha_0}\right)^2\right]^{-1/2}. \tag{2.76}$$

In this case we have a five-parametric family of profiles $y = \omega_0(x)$. It is described by

$$\omega_0(x) = \begin{cases} y_0 + \beta_0\sqrt{1 - [(x - x_0)/\alpha_0]^2}, & x_2 \le x \le b, \\ d(x - x_2) + y_2, & 0 \le x \le x_2. \end{cases} \tag{2.77}$$

The free parameters are b, h, γ_0, β_0 and x_2, and the other parameters are expressed through them by

$$x_0 = b - \gamma_0, \quad y_0 = h - \beta_0, \quad \alpha_0 = \gamma_0\beta_0[h(2\beta_0 - h)]^{-1/2}. \tag{2.78}$$

In the second case the profile is given by

$$\omega_0(x) = \begin{cases} y_0 + \beta_0\sqrt{1 - [(x - x_0)/\alpha_0]^2}, & x_0 \le x \le b, \\ h, & 0 \le x \le x_0, \end{cases} \tag{2.79}$$

Now there are four free parameters, b, h, γ_0 and β_0. The fore part is described by the same arc as before with $x_2 = x_0$, and the straight part of the profile is parallel to the x-axis, $0 \le x \le x_0 = b - \gamma_0$, $y = h$.

The third profile has the same fore part as in case 2, while the rest of the profile is described by a parabola,

$$\omega_0(x) = \begin{cases} y_0 + \beta_0\sqrt{1 - [(x - x_0)/\alpha_0]^2}, & x_0 \le x \le b, \\ -(h - h_1)(x/x_0)^2 + 2(h - h_1)x/x_0 + h_1, & 0 \le x \le x_0, \end{cases} \tag{2.80}$$

The five parameters b, h, γ_0, β_0, and $h_1 \in (0, h)$ are free, while the others, x_0, y_0, and α_0 are given by (2.78). The function $\omega(x)$ is convex, continuously-differentiable at the point $x = x_0$ and has a positive derivative for $0 \le x < x_0$.

For computations of the normal traction $\sigma_y(x, 0)$, we selected the following values of the problem parameters: $\nu = 0.3$, $b = 20$, $h = 1$, $\mu = 1$, $\sigma = V/c_s = 0.5$, $k = 0.3$, and the fore crack-like cavity

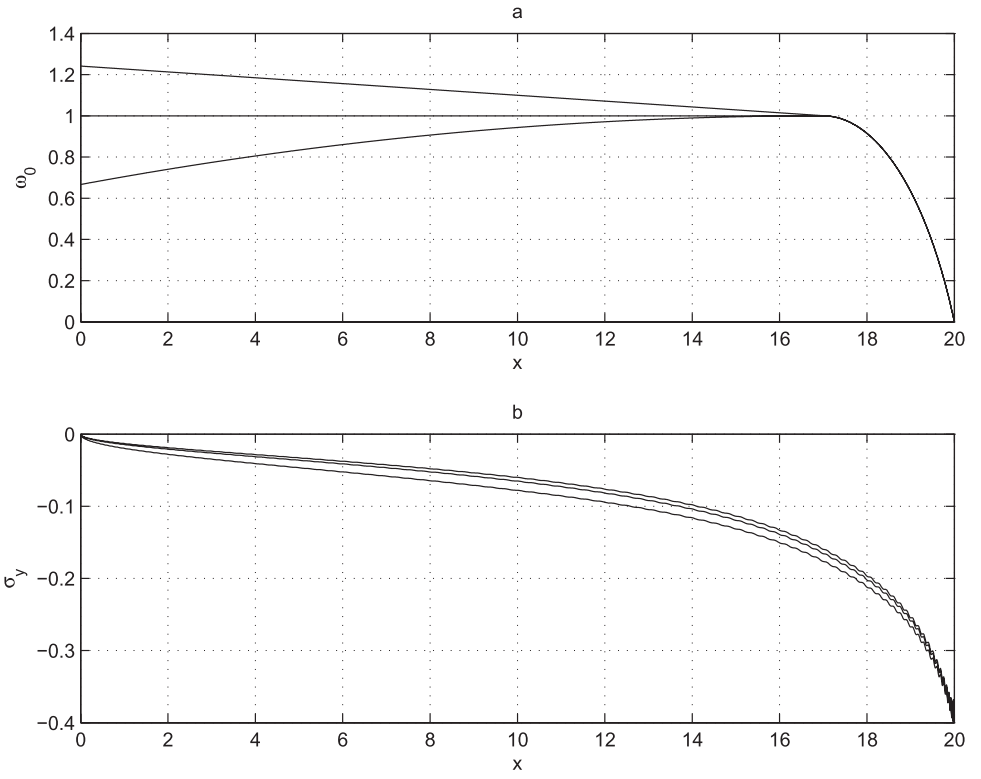

Fig. 3 The traction $\sigma_y(x, 0)$ acting on the body surface when $\gamma_0 = 3$, $\beta_0 = 2$, $x_2 = 1.005x_0$ and $h_1 = \frac{2}{3}h$ and when there is a fore crack-like cavity of length $l = 1$. The upper, middle, and lower traction curves in the lower diagram correspond to the upper, middle and lower samples of the body profile in the upper diagram

length $l = b_0 - b = 1$. Shown in Figs. 3 and 4 are the normal traction $\sigma_y(x, 0)$ for $x \in [0, b]$ for some body profiles. These diagrams demonstrate that the normal traction σ_y is negative and pressure is positive everywhere in the contact zone. The same pattern is revealed for similar profiles with a crack-like cavity ahead of the body. This determines the choice of the parameters $b_- = 0$ and $b_+ = b$; it has been proved that the traction components $\sigma_y(x, 0)$ and $\tau_{xy}(x, 0) = k\sigma_y(x, 0)$ vanish for any choice of the parameters b_- and b_+. Analysis of the numerical results reveal large deviations of the traction components in a small neighborhood of the point $b_+ = b$ (the first derivative of $\partial\sigma_y(x, 0)/\partial x$ has a power singularity at this point).

In Fig. 5, the variation of the resistance force F with the speed parameter $\sigma = V/c_s$ is demonstrated for the three profiles used in Fig. 3a when $\gamma_0 = 3$, $\beta_0 = 2$, $x_2 = 1.005x_0$, $h_1 = \frac{2}{3}h$, $l = 1$ and $k = 0.3$. It is seen that the force F decreases as the speed approaches the Rayleigh speed c_R. The solid lines correspond to the resistance force computed by formula (2.55) for the profiles given by (2.77), (2.79) and (2.80). The dash lines are the corresponding graphs of the resistance force computed according to the formula

$$F = -2\int_{b_-}^{b_+} \tau_{xy} dx \tag{2.81}$$

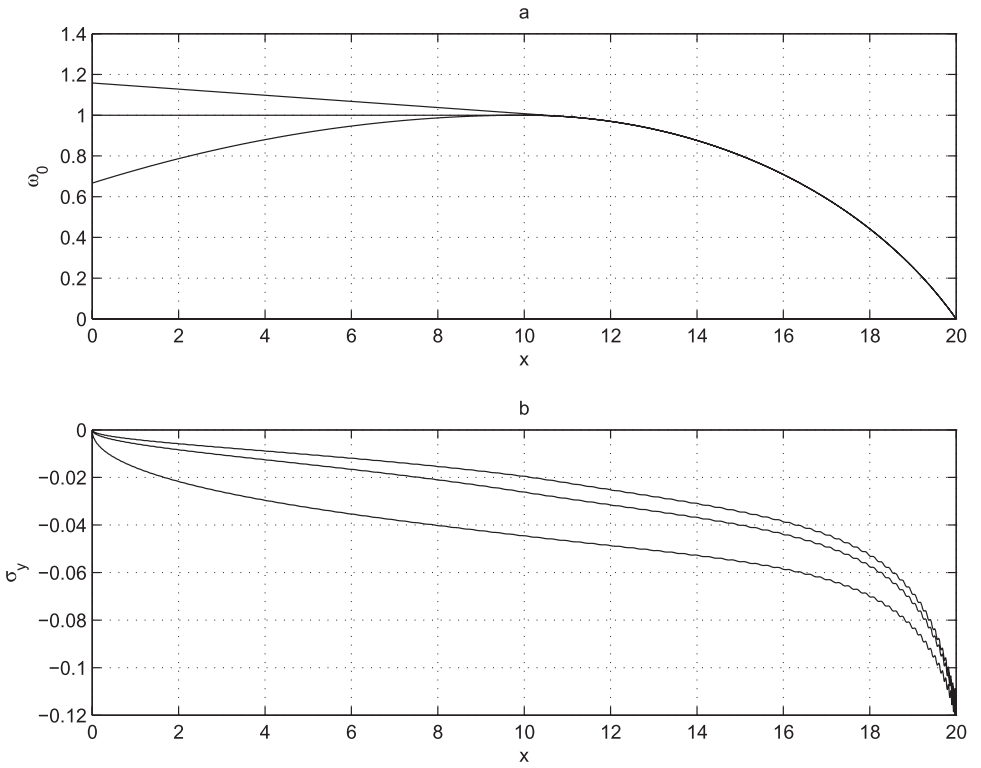

Fig. 4 The traction $\sigma_y(x, 0)$ acting on the body surface when $\gamma_0 = 10$, $\beta_0 = 2$, $x_2 = 1.1x_0$ and $h_1 = \frac{2}{3}h$, and when there is a fore crack-like cavity of length $l = 1$. The upper, middle and lower traction curves in the lower diagram correspond to the upper, middle and lower samples of the body profile in the upper diagram

that neglects the stress σ_x. As it becomes evident formula (2.81) leads to the unrealistic zero value of the resistance force as $V = c_R$.

Figure 6a illustrates the dependence of the fore crack length $l = b_2 - b$ on the speed parameter V/c_s when $k = 0.3$ for some body profiles. The parameter l is recovered from the transcendental equation (2.49). To select the Griffith material constant T, we assume that at speed $V = 0.5c_s$ a fore crack has length 1 that is $b_0 = 21$. Then from (2.48) the constant T is computed as

$$T = \frac{V^2 K_I^2 a_l}{4c_s^2 \mu R} = 0.51914224526. \tag{2.82}$$

This constant was used to determine from the transcendental equation (2.49) the fore crack length $l = b_0 - b$ when speed V varies from 0 to c_R. In Fig. 6b, we show the variation of the resistance force F with V/c_s when $k = 0.3$ and the crack-like cavity length $l(V/c_s)$ is determined by (2.49). The lower, middle and upper curves correspond to the upper, middle and lower samples of the body profile shown in Fig. 3a, respectively.

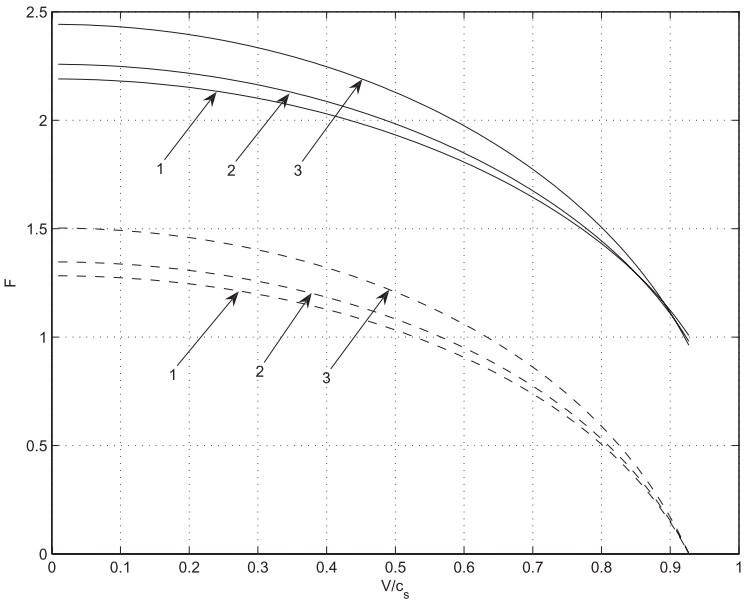

Fig. 5 The resistance force F versus V/c_s when $k = 0.3$ and there is a fore crack-like cavity of length $l = 1$. The curves 1, 2 and 3 correspond to the upper, middle and lower samples of the body profile shown in Fig. 3a. The solid and dash lines are the graphs of the resistance force computed by formulas (2.55) and (2.81), respectively

Shown in Fig. 7a and b are the fore crack length l and the resistance force F as a function of the friction coefficient k when $V/c_s = 0.5$. The Griffith material constant T was assumed to be the same as in Fig. 6a and b. The lower, middle and upper curves correspond to the upper, middle and lower body profile shown in Fig. 3a, respectively.

3. Motion of a thin body when there is no cavity ahead

In this section, we aim to analyze an alternative model of rapid penetration of a thin rigid body when there is a semi-infinite crack-like cavity behind the body but no cavity ahead, that is $b_+ = b_0 = b$. The body is symmetric with respect to the plane of motion, and, in the moving coordinates $x = x_1 - Vt$ and $y = x_2$, the boundary conditions of the model are given by

$$\begin{aligned} \sigma_y = 0, \quad \tau_{xy} = 0, \quad -\infty < x < 0, \\ \tau_{xy} = k\sigma_y, \quad u_{y,x} = \omega(x), \quad b_- < x < b, \\ \tau_{xy} = 0, \quad u_{y,x} = 0, \quad b < x < +\infty. \end{aligned} \tag{3.1}$$

As in the previous section, the new model is governed by two Riemann–Hilbert problem of the form (2.14) and (2.15). However, now the first problem (2.14) has a new coefficient. It is

$$G(x) = \begin{cases} -(p - iq)/(p + iq), & b_- < x < b, \\ -1, & -\infty < x < b_-, \\ 1, & b < x < +\infty. \end{cases} \tag{3.2}$$

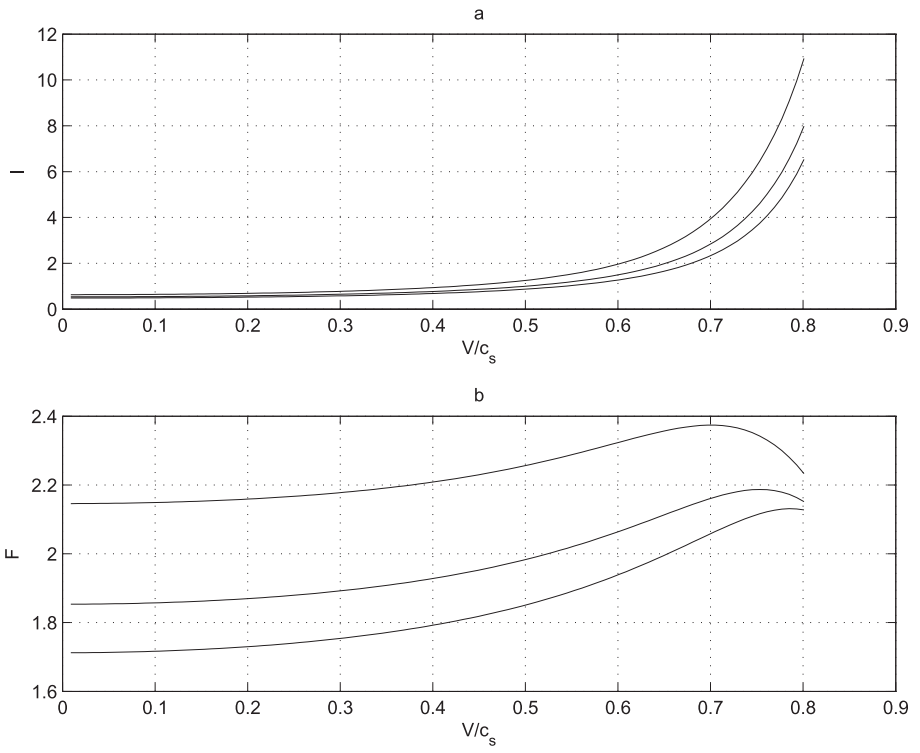

Fig. 6 (a) The crack-like cavity length $l = b_2 - b$ ($b_- = 0$, $b_+ = b$) versus the speed parameter V/c_s when $k = 0.3$. (b) The resistance force F versus V/c_s when $k = 0.3$ and the crack-like cavity length $l(V/c_s)$ is defined by equation (2.49). The lower, middle and upper curves in diagrams (a) and (b) correspond to the upper, middle and lower samples of the body profile shown in Fig. 3a, respectively

The function $G(x)$ can symmetrically be factorized by means of the function

$$X(z) = (z - b_-)^{\kappa}(z - b)^{1/2-\kappa}, \tag{3.3}$$

where κ is the parameter introduced in (2.19), and the branches of the power functions are fixed by the conditions (2.20) in the plane cut along the ray $\{-\infty < x < b, y = 0\}$. It is directly verified that the function $X(z)$ solves the factorization problem (2.17) for the new coefficient $G(x)$.

The solution of the Riemann–Hilbert problems, the functions $\Omega_1(z)$ and $\Omega_2(z)$, are given by formulas (2.26) and (2.28) where $X(z)$ needs to be replaced by the function (3.3). This results in the following formula for the normal traction component:

$$\sigma_y(x, 0) = -\frac{\mu R}{p^2 + q^2}\left[p\omega(x) - \frac{q}{\pi}(x - b_-)^{\kappa}(b - x)^{1/2-\kappa} I(x)\right], \tag{3.4}$$

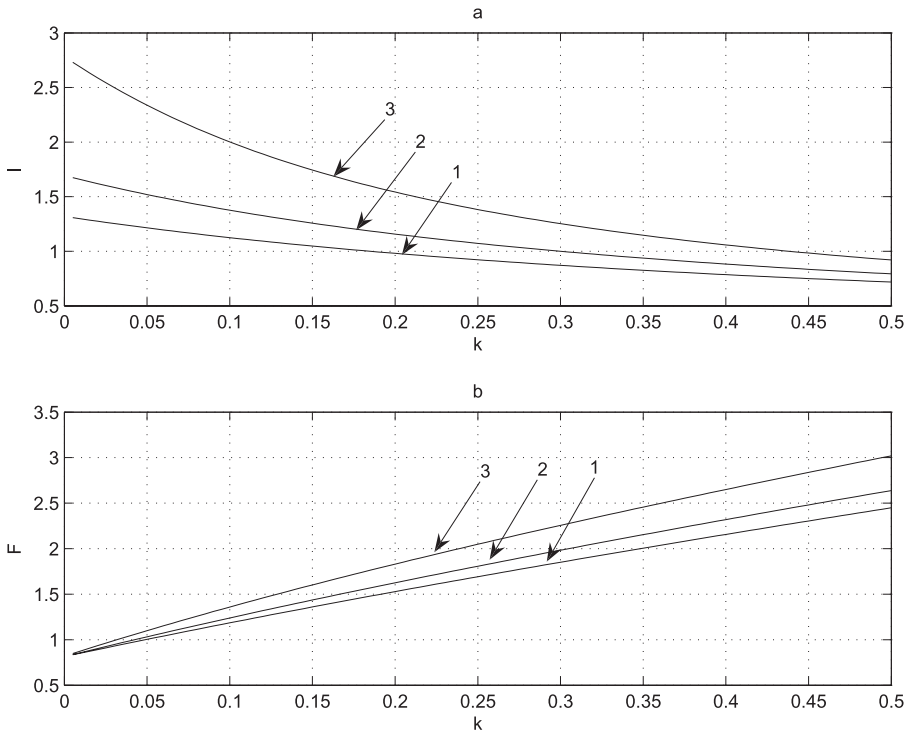

Fig. 7 (a) The crack-like cavity length l versus the friction coefficient k when $V/c_s = 0.5$. (b) The resistance force F versus k when $V/c_s = 0.5$ and the crack-like cavity length $l(V/c_s)$ is defined by equation (2.49). Curves 1, 2 and 3 correspond to the upper, middle and lower samples of the body profile shown in Fig. 3a

where

$$I(x) = \int_{b_-}^{b_+} \frac{\omega(\xi)d\xi}{(\xi - b_-)^{\kappa}(b - \xi)^{1/2-\kappa}(\xi - x)}. \tag{3.5}$$

This integral can be computed in the same way as the integral (2.59) if instead of the function (2.60) we take

$$f(\tau) = \sqrt{1 - \tau}\,\omega((b - b_-)\tau + b_-). \tag{3.6}$$

Then employing the expansion (2.62) that is

$$\sqrt{\frac{b - x}{b - b_-}}\,\omega(x) = \sum_{n=0}^{\infty} f_n P_n^{-\kappa,\kappa-1}\left(\frac{b^+ - x}{b^-}\right), \tag{3.7}$$

and the relation (2.63) we eventually derive from (3.4) that the normal traction $\sigma(y)(x, 0)$ vanishes at the points $x = b$ and $x = b_-$ (regardless of the choice of the point $b_- \in [0, b)$. The function $\sigma_y(x, 0)$ has the form

$$\sigma_y(x, 0) = -\frac{\mu R q (x - b_-)^{\kappa}(b - x)^{1/2-\kappa}}{\sqrt{b - b_-}(p^2 + q^2)\sin\pi\kappa} \sum_{n=1}^{\infty} f_n P_{n-1}^{\kappa,1-\kappa}\left(\frac{b^+ - x}{b^-}\right), \quad b_- < x < b. \tag{3.8}$$

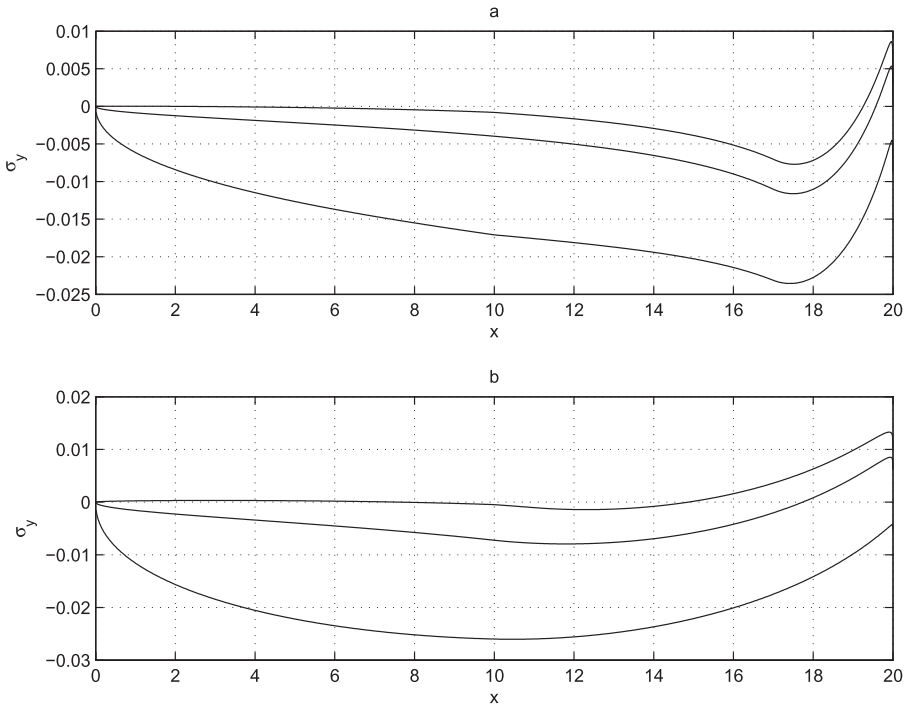

Fig. 8 The traction $\sigma_y(x, 0)$ acting on the body surface when there is no fore cavity in the case $\beta_0 = 2, h_1 = \frac{2}{3}h$, $V/c_s = 0.5$, and $k = 0.3$. The upper, middle and lower traction curves in diagrams a and b correspond to the upper, middle and lower samples of the body profile shown in Fig. 3a with $\gamma_0 = 3$, $x_2 = 1.003x_0$ and Fig. 3b with $\gamma_0 = 10$, $x_2 = 1.1x_0$, respectively

Numerical results for the contact stress σ_y presented in Fig. 8a and b were obtained for the following parameters: $\nu = 0.3$, $b = 20$, $h = 1$, $\mu = 1$, $\sigma = V/c_s = 0.5$ and $k = 0.3$ for the profiles employed in Figs. 3 and 4. The upper curve in Fig. 8a corresponds to the case $x_2 = 1.003x_0$. It turns out that for bodies whose rear part $0 \le x \le x_2$ is described by the linear function $d(x - x_2) + y_2$ with $x_2 > x_0$, $d < 0$, and y_2 given is by (2.76) the normal traction component may become positive in the rear part of the body surface. For sufficiently big deviation of the rear profile from the line $y = h$ $\sigma_y > 0$, and the pressure distribution is negative. In this case, the model is not applicable since the Coulomb friction boundary condition does not valid. Also, there is a small area in the fore part of the body surface where $\sigma_y > 0$ (Fig. 8a and b). This indicates that for such profiles there is a cavity ahead of the body. At the same time, for profiles of type 3 described by (2.80) the normal traction σ_y is negative everywhere in the body surface, and there is full contact between the rigid body and the elastic medium.

Figures 9 and 10 present the variation of the resistance force F with the speed parameter V/c_s and the friction coefficient k, respectively. The resistance force was computed according to the formula

$$F = 2\int_{b'}^{b''} (\omega\sigma_x - \tau_{xy})dx \tag{3.9}$$

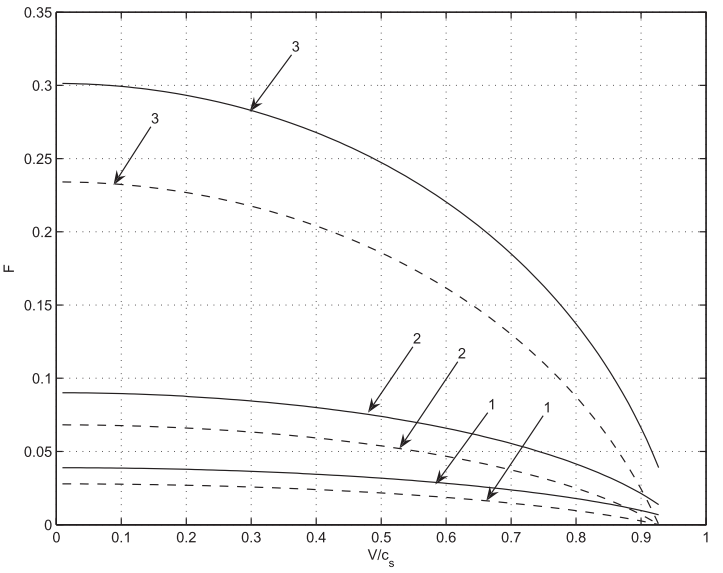

Fig. 9 The resistance force F versus V/c_s when $k = 0.3$ and there is no fore cavity. The curves 1, 2, and 3 correspond to the upper, middle and lower samples of the body profile shown in Fig. 3a, respectively, with $\gamma_0 = 3$ and $x_2 = 1.003x_0$. The solid and dash lines are the graphs of the resistance force computed by formula (3.9) with and without σ_x, respectively

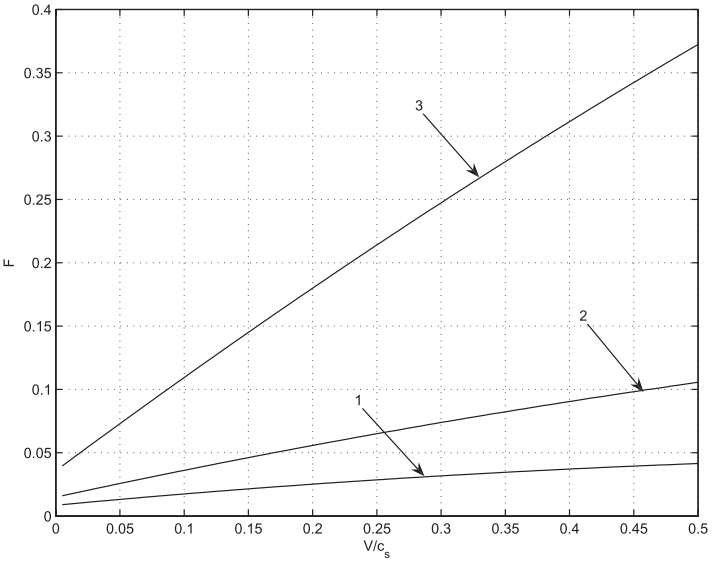

Fig. 10 The resistance force F versus the friction coefficient k when $V/c_s = 0.5$ and there is no fore cavity. The curves 1, 2 and 3 correspond to the upper, middle and lower samples of the body profile shown in Fig. 3a with $\gamma_0 = 3$ and $x_2 = 1.003x_0$

with (b', b'') being the interval where the traction σ_y is negative (the actual contact zone). As in the previous model with a crack-like cavity ahead of the body, the largest resistance force is for type 3 profiles and the smallest one is for type 1 profiles given by (2.80) and (2.77), respectively. As in Model 1, the negligence of the stress σ_x in formula (3.9) for the resistance force leads to the unrealistic zero value of the resistance force when speed reaches the Rayleigh speed. It is seen from Fig. 10 that friction affects the resistance force more for profiles of type 3 than for profiles of type 1.

4. Conclusions

In this work, we have analyzed two steady-state models of penetration of a thin finite rigid body in an infinite elastic medium. Both models assume that the body and the medium contact according to the Coulomb friction law, and the body leaves a semi-infinite crack-like cavity behind. The difference between the two models is the presence of a fore finite crack-like cavity in Model 1 and its absence in Model 2. Both model problems have been reduced to two sequently solved Riemann–Hilbert problems. Analysis of the solution obtained by quadratures shows that the normal and tangential traction components and the normal velocity vanish at the separation points selected arbitrarily. We have identified the aft and fore separation points as the points where the normal traction component ceases to be compressive and becomes tensile. It turns out that for profiles studied in Model 1 with a fore crack the medium does not separate from the body, while in Model 2, when there is no crack ahead, separation of the medium may or may not occur.

We have proposed an integral formula for the resistance force which takes into accounts not only the tangential stress τ_{xy} but also the stresses σ_x and σ_y. The resistance force is eventually expressed as the integral over the upper contact area of the function $2(\omega\sigma_x - \tau_{xy})$, where $\omega(x)$ is the slope of the profile of the body. We have discovered that the disregarding the stress σ_x in the resistance force formula underestimates its values and leads to the unrealistic zero value as speed reaches the Rayleigh speed.

Numerical results have shown that for ogive-nose thin two-dimensional penetrators with a semi-infinite trailing cavity and with or without a fore crack-like cavity the resistance force varies significantly with motion speed. If the fore crack length is fixed (zero for Model 2 and positive for Model 1) and assumed to be independent of speed, then similarly to the variation of the Mode-I SIF with sub-Rayleigh speed in dynamic fracture the resistance force is a decreasing function of speed. If the fore crack length in Model 1 is recovered from the Griffith criterion as the root of the associated transcendental equation, then the crack length is an increasing function of speed, while the resistance force depends on speed not monotonically. It attains its maximum at a certain speed and then decreases as speed approaches the Rayleigh speed.

Challenging and important for applications are the transient and three-dimensional axisymmetric models. By using the solution for the transient model and the nonuniform speed crack propagation algorithm (**10**, **14**) it may be possible to analyze nonuniform speed motion of a rigid body in an elastic medium.

Acknowledgements

Research was sponsored by the Army Research Office and was accomplished under Grant Number (W911NF-17-1-0157). The views and conclusions contained in this document are those of the author and should not be interpreted as representing the official policies, either expressed or implied, of the

Army Research Office or the U.S. Government. The U.S. Government is authorized to reproduce and distribute reprints for Government purposes notwithstanding any copyright notation herein.

References

1. G. I. Barenblatt and G. P. Cherepanov, On the wedging of brittle bodies, *J. Appl. Math. Mech.* **24** (1960) 993–1014.

2. G. I. Barenblatt and R. V. Goldstein, Wedging of an elastic body by a slender wedge moving with a constant super-Rayleigh subsonic velocity, *Int. J. Fracture Mech.* **8** (1972) 427–434.

3. I. V. Simonov, Transonic flow of an elastic medium past a thin solid, *J. Appl. Math. Mech.* **48** (1984) 74–81.

4. A. V. Zvyagin, Motion of a body in an elastic medium with friction, *Vestnik Moskov. Univ. Ser. I Mat. Mekh.* **5** (2006) 44–50.

5. A. V. Zvyagin, Supersonic motion of a rigid body in an elastic medium with friction, *Vestnik Moskov. Univ. Ser. I Mat. Mekh.* **4** (2007) 52–61.

6. W. Goldsmith, Review: non-ideal projectile impact on targets, *Int. J. Impact. Engng.* **22** (1999) 95–395.

7. G. H. Jones and J. A. Zukas, Mechanics of penetration: analysis and experiment, *Int. J. Engn. Sci.* **16** (1978) 879–903.

8. K. B. Broberg, *Cracks and Fracture* (Academic Press, San Diego 1999).

9. Y. A. Antipov, Subsonic semi-infinite crack with a finite friction zone in a bimaterial, *J. Mech. Phys. Solids* **57** (2009) 1934–1957.

10. L. B. Freund, *Dynamic Fracture Mechanics* (Cambridge University Press, Cambridge 1990).

11. F. D. Gakhov, *Boundary Value Problems* (Pergamon Press, Oxford 1966).

12. J. R. Willis, A comparison of the fracture criteria of Griffith and Barenblatt, *J. Mech. Phys. Solids* **15** (1967) 151–162.

13. F. G. Tricomi, On the finite Hilbert transformation, *Quart. J. Math.* **2** (1951) 199–211.

14. Y. A. Antipov and A. V. Smirnov, Fundamental solution and the weight functions of the transient problem on a semi-infinite crack propagating in a half-plane, *Z. Angew. Math. Mech. (ZAMM)* **96** (2016) 1156–1174.